Hole Spectral Function and 2p1h Response Propagator.

Rijsdijk, G.A.; Geurts, W.J.W.; Allaart, K.; Dickhoff, W.H.

published in
Physical Review C
1996

DOI (link to publisher)
10.1103/PhysRevC.53.201

document version
Publisher's PDF, also known as Version of record

Hole spectral function and two-particle–one-hole response propagator

G. A. Rijsdijk, W. J. W. Geurts, and K. Allaart
Department of Physics and Astronomy, Free University, De Boelelaan 1081, 1081 HV Amsterdam, The Netherlands

W. H. Dickhoff
Department of Physics, Washington University, St. Louis, Missouri 63130
(Received 1 August 1995)

The fragmentation of one-nucleon knock-out strength at low energies is considered from the viewpoint of the two particle-one hole (and two hole- one particle) response propagator. The aim is to deal with particle-particle (and hole-hole) as well as particle-hole collectivity simultaneously. This is achieved on a Tamm-Dancoff level by the so-called Faddeev approximation of the $2p1h$ propagator. Results of this approach illustrate the relevance of this consistent treatment of both particle-particle (hole-hole) and particle-hole collectivity. A further extension, within the framework of $2p1h$ RPA which was sometimes applied in the past, has serious unsolved problems, some of which are discussed in detail.

PACS number(s): 25.40.Kv, 21.10.Jx, 21.60.Jz, 24.10.Cn

I. INTRODUCTION

Shell model properties of nuclei have been studied in detail recently by means of proton knockout reactions with electron beams. By measuring the momentum dependence of the cross section for discrete final states, a direct confirmation is found that nucleons are residing in the various shell model orbits [1–5]. Moreover, one demonstrates that the energies of the final states, corresponding to the knockout from a specific bound orbital, exhibit a spreading which may be related to properties of the optical potential for scattering states [6–9]. Some uncertainty still remains about the absolute values of the spectroscopic factors deduced from the analysis of the data and therefore also about the occupation probabilities of the various shell model orbits. There is some consensus that these occupation probabilities of orbitals just below the Fermi energy are about 0.75 [4,10]. On the other hand, the analysis of just the $(e,e'p)$ data shows some dependence on optical potentials used and on whether or not a relativistic nuclear model is adopted [11].

Theoretical calculations of the spectroscopic strength have been performed dealing with two different aspects. First, shell model orbits will be depleted due to the short-range repulsion. This effect is sometimes represented by the introduction of correlation functions in a Slater determinant [12]. The short-distance binary collisions will be sensitive to hardly any other nuclear structure than just the local density. Therefore the depletion of states below the Fermi level as well as the complete spectral function has been studied in nuclear matter at various densities, both by Green function methods [13,14] and with variational correlation functions [15,16]. Finally, the spectral function in ^{16}O has been calculated in a Brueckner Hartree-Fock approach [17]. Nuclear matter results have also been folded into phenomenological model calculations for finite nuclei [18]. Somewhat depending on the methods and interactions used, one finds a 10–20 % depletion of the orbits due to the short-range forces. Since the dominant mechanism dealt with in these calculations is the hard binary collision, the occurrence of particles with large (relative) momenta is implicit. When one of these is knocked out, the residual nucleus is left behind with an excitation energy of 100 MeV and higher [17]. This has to be verified by $(e,e'p)$ reactions with high missing momentum and energy. Additional and more direct information may be obtained by detection of pairs with high relative momenta and for low excitation energy of the final nucleus with two nucleons fewer [19,20].

Besides the strongly repulsive short-range correlations, there are also the long-range correlations assiocated with the shell structure and the surface of the nucleus which contribute to the depletion of shell model orbits. These long-range correlations are responsible for the fragmentation of knock-out strength at low excitation energies of the final system, up to about 50 MeV [9,21,22]. Theoretically, these long-range correlations may be taken into account by solving the Dyson equation with a self-energy in some approximation beyond the static (Brueckner) Hartree-Fock potential. Dispersion and correlation effects have been included by various authors [9,21] in the form of dynamical contributions to the self-energy of second order in an effective interaction, e.g., a G matrix. Results of such calculations account rather well for the overall spreading width of deeply bound states. On the other hand, the weaker fragments for discrete states at low energy are considerably underestimated. Higher order contibutions to the self-energy, in the form of a coupling of particle or hole motion to collective modes, may be the explanation for this. Attempts in this direction were made in Ref. [22], in which particle pairs and hole pairs as well as particle-hole pairs in the self-energy were treated in the Tamm-Dancoff approximation (TDA) or random-phase approximation (RPA). These calculations were still unsatisfactory in some respects, however. First, there was some violation of the Pauli principle, as is also implicit in phenomenological particle-phonon models. In the calculation of the collective phonon the presence of the particle or hole is ignored. Second, the method was not suitable to treat particle-particle and hole-hole correlations simultaneously with particle-hole correlations.

It is the aim of the present paper to develop a method which addresses these problems and to see how relevant this

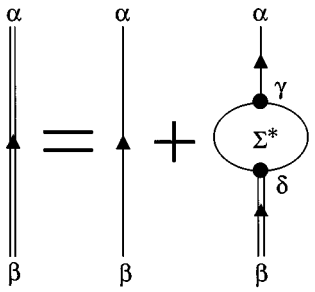

FIG. 1. Graphical representation of the Dyson equation (5). The double line represents the full propagator $g(\omega)$; the single line the free propagator $g^{(0)}(\omega)$ of a nucleon in a suitably chosen mean-field potential.

simultaneous treatment of both types of correlations is. This is most conveniently done by connecting the self-energy to the two-particles–one-hole ($2p1h$) response propagator. In Sec. II this formalism will be presented. Two approximations for the $2p1h$ response propagator, the Tamm-Dancoff and random-phase approximations, will be considered in Secs. II B and II C, respectively. Applications for the nuclei ^{48}Ca and ^{90}Zr are discussed in Sec. III. Section IV contains some conclusions.

II. FORMALISM

A. Spectral function and self-energy

The present work is an extension of Ref. [9] in which the reader may find a more extensive discussion of the computational techniques. The quantity of interest is the hole spectral function

$$S_h(\alpha,\omega)=\sum_{n=0}|\langle\Psi_n^{A-1}|a_\alpha|\Psi_0^A\rangle|^2\delta(\omega-(E_0^A-E_n^{A-1})), \tag{1}$$

which represents the probability density for removing a nucleon from the orbit α from the ground state of the nucleus with A nucleons while ending up in the nth state of the $A-1$ system with energy E_n^{A-1} ($n=0$ denotes the ground state). The occupation probability of the orbit α is obtained by integration of the hole spectral function

$$n_\alpha=\int_{-\infty}^{\varepsilon_F^-}d\omega S_h(\alpha,\omega), \tag{2}$$

with an upper limit of integration $\varepsilon_F^-=E_0^A-E_0^{A-1}$. The spectral function can be calculated from the imaginary part of the single-particle (SP) propagator or Green function,

$$S_h(\alpha,\omega)=\lim_{\eta\to0}\frac{1}{\pi}\mathrm{Im}g_{\alpha\alpha}(\omega),\quad \omega<\varepsilon_F^-, \tag{3}$$

by using the spectral or Lehmann representation of the SP propagator which is given by

$$g_{\alpha\beta}(\omega)=\sum_n\frac{\langle\Psi_0^A|a_\alpha|\Psi_n^{A+1}\rangle\langle\Psi_n^{A+1}|a_\beta^\dagger|\Psi_0^A\rangle}{\omega-(E_n^{A+1}-E_0^A)+i\eta}$$

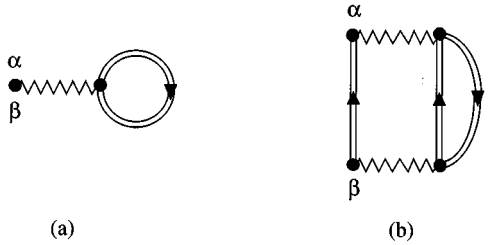

FIG. 2. First and second order diagrams that contribute to the irreducible self-energy Σ^* in Eq. (5). The lines represent the single-pole approximation (6) to the Green function, with diagram (a) already taken into account. Diagram (b) then represents Eq. (10). Interaction lines represent a G-matrix interaction used in this work.

$$+\sum_m\frac{\langle\Psi_0^A|a_\beta^\dagger|\Psi_m^{A-1}\rangle\langle\Psi_m^{A-1}|a_\alpha|\Psi_0^A\rangle}{\omega-(E_0^A-E_m^{A-1})-i\eta}. \tag{4}$$

This Green function also contains information on the process of adding a particle (see Ref. [9]) which illustrates that the SP strength that is not seen in removal experiments must be present in particle addition experiments. The SP propagator satisfies the well-known Dyson equation [23,24]

$$g_{\alpha\beta}(\omega)=g_{\alpha\beta}^{(0)}(\omega)+\sum_{\gamma\delta}g_{\alpha\gamma}^{(0)}(\omega)\Sigma_{\gamma\delta}^*(\omega)g_{\delta\beta}(\omega), \tag{5}$$

which is graphically represented in Fig. 1. In this equation $g^{(0)}$, depicted by a single line in the figure, is the Green function of a freely propagating particle or hole in a suitably chosen mean-field potential. The irreducible self-energy Σ^* in Eq. (5) may be written as an infinite series of successively higher order terms in the interaction, minus the interaction already included in the mean field of $g^{(0)}$. In practice, the series expansion of Σ^* has to be truncated at some point, which implies a corresponding approximation of the spectral function. The lowest two orders in the interaction are represented in the diagrams of Fig. 2. The lowest order diagram, Fig. 2(a), generates the self-consistent Hartree-Fock (HF) field. Assuming that this is just the part of the interaction already absorbed in $g^{(0)}$, this implies

$$g_{\alpha\beta}^{(1)}(\omega)=\delta_{\alpha\beta}\left[\frac{\theta(\alpha-F)}{\omega-\varepsilon_\alpha^{\mathrm{HF}}+i\eta}+\frac{\theta(F-\alpha)}{\omega-\varepsilon_\alpha^{\mathrm{HF}}-i\eta}\right], \tag{6}$$

where θ is the step function which indicates whether the orbit α is above or below the Fermi level and corresponds to HF quantum numbers.

The second order term $\Sigma^{*(2)}$ is displayed in Fig. 2(b). When this term is included in the Dyson equation one has to solve the coupled equations

$$g_{\alpha\beta}^{(2)}(\omega)=g_{\alpha\beta}^{(1)}(\omega)+\sum_{\gamma\delta}g_{\alpha\gamma}^{(1)}(\omega)\Sigma_{\gamma\delta}^{*(2)}(\omega)g_{\delta\beta}^{(2)}(\omega) \tag{7}$$

and

$$\Sigma^{*(2)}_{\alpha\beta}(\omega)=\frac{1}{2}\sum_{\mu\nu\kappa\lambda\gamma\delta}\int\frac{d\omega_1}{2\pi i}\int\frac{d\omega_2}{2\pi i}\{\langle\alpha\delta|V|\mu\kappa\rangle\langle\nu\lambda|V|\beta\gamma\rangle g^{(2)}_{\mu\nu}(\omega-\omega_1+\omega_2)g^{(2)}_{\kappa\lambda}(\omega_1)g^{(2)}_{\gamma\delta}(\omega_2)\}. \tag{8}$$

In Ref. [9] a single-pole approximation

$$g^{(2)}_{\alpha\beta}\approx\delta_{\alpha\beta}\left[\frac{\theta(\alpha-F)}{\omega-\varepsilon_\alpha+i\eta}+\frac{\theta(F-\alpha)}{\omega-\varepsilon_\alpha-i\eta}\right] \tag{9}$$

was substituted in expression (8) for the second order self-energy. The values ε_α of the pole energies of shells close to the Fermi level were matched in Ref. [9] with the exprimental energies of the states with largest spectroscopic factor for each j^π value. For more remote shells (estimated) mean removal energies are identified with ε_α. With the approximation (9) the self-energy (8) takes the approximate form

$$\Sigma^{*(2)}_{\alpha\beta}(\omega)\approx\frac{1}{2}\sum_{\mu\nu\kappa}\langle\alpha\kappa|V|\mu\nu\rangle\langle\mu\nu|V|\beta\kappa\rangle\left\{\frac{\theta(\mu-F)\theta(\nu-F)\theta(F-\kappa)}{\omega-(\varepsilon_\mu+\varepsilon_\nu-\varepsilon_\kappa)+i\eta}+\frac{\theta(F-\mu)\theta(F-\nu)\theta(\kappa-F)}{\omega-(\varepsilon_\mu+\varepsilon_\nu-\varepsilon_\kappa-i\eta}\right\} \tag{10}$$

and the Dyson equation (7) is then solved with this approximate form by the procedure sketched in Ref. [9]. It should be noted that the use of a realistic G-matrix interaction in the second order self-energy implies that only a limited domain of the configuration space can be included before double counting becomes a serious problem. Using a phenomenological interaction as in Ref. [21], the choice of the configuration space is arbitrary. In Ref. [21] approximation (9) was avoided and complete self-consistency was obtained, although the fragmentation of strength in the low energy region was also not completely satisfactory. In both Refs. [9] and [21] it was therefore suggested that collective correlations among the propagating lines in diagram 2(b), i.e., in $2p1h$ and $1p2h$ states, should be included in order to account for the collectivity of the phonons to which the particle or hole couples. It is this kind of extension that will be considered in the following.

B. Self-energy in a "Faddeev" approximation

In earlier work [22] the Dyson equation for the single-particle propagator was solved for a number of approximations for the self-energy Σ^*. These were presented as "tractable" extensions of the second order self-energy, represented by the Goldstone diagrams in Figs. 3(a), 3(b). The freely propagating pair of particles or holes in diagrams 3(a), 3(b) was replaced by the Tamm-Dancoff approximation or random-phase approximation for the particle-particle propagator [diagrams 3(c), 3(d)]. Similarly, the freely propagating particle-hole pair can be replaced by the TDA- or RPA-correlated particle-hole propagator [diagrams 3(e), 3(f)].

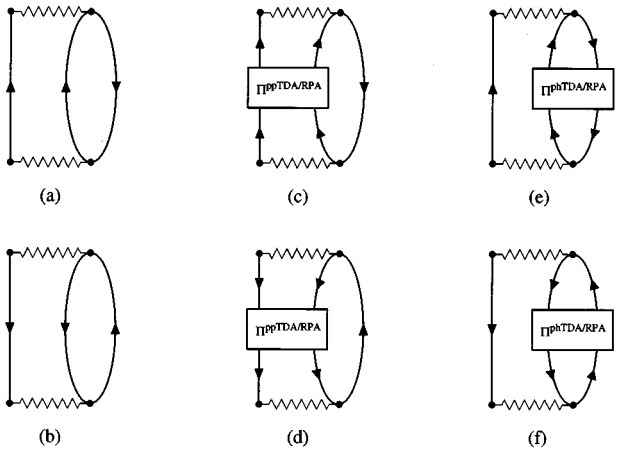

FIG. 3. Second order self-energy terms represented by Goldstone diagrams (a) and (b). Extensions applied in [22] are made by including TDA or RPA correlations in the particle-particle [diagrams (c) and (d)] or particle-hole channel [diagrams (e) and (f)].

In order to arrive at an approximation for Σ^* in which correlations among all three propagating lines are included, one needs a more formal treatment of the relation between the self-energy and higher-point Green functions, especially the two-particle–one-hole propagator. These relations are derived by differentiating the SP propagator

$$ig_{\alpha\beta}(t-t')=\langle\Psi^A_0|T[c_\alpha(t)c^\dagger_\beta(t')]\Psi^A_0\rangle, \tag{11}$$

with respect to the time arguments, which will relate the SP propagator to the two-particle propagator. This scheme can be continued and leads to a set of coupled equations, in

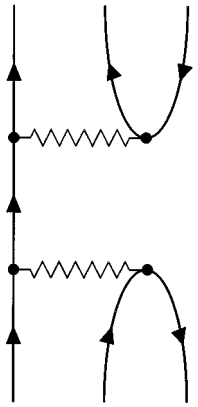

FIG. 4. Lowest order reducible contribution to the $2p1h$ propagator.

which the n-body propagator is related to the $(n+1)$-body propagator and so on [25].

To avoid extensive formal development we will not carry out this procedure here, but instead give a less formal derivation of the relation between the self-energy and the $2p1h$ propagator, which will suit the aims of this investigation. This result can be found by inspection of the mth order term of the perturbation expansion for $g_{\alpha\beta}(t-t')$ for $m \geqslant 2$,

$$ig^{(m)}_{\alpha\beta}(t-t') = \frac{(-i)^m}{m!}\int_{-\infty}^{\infty} dt_1 \cdots \int_{-\infty}^{\infty} dt_m \Bigg\langle \Phi_0 | T\Bigg[H_1(t_1)\cdots H_1(t_{m-2}) \sum_{klmn} \frac{1}{4} V_{klmn} c_k^\dagger(t_{m-1}) c_l^\dagger(t_{m-1}) c_n(t_{m-1}) c_m(t_{m-1}) \times \sum_{pqrs} \frac{1}{4} V_{pqrs} c_p^\dagger(t_m) c_q^\dagger(t_m) c_s(t_m) c_r(t_m) c_\alpha(t) c_\beta^\dagger(t') \Bigg] | \Phi_0 \Bigg\rangle, \tag{12}$$

in which two of the interactions H_1 are written out explicitly. Contraction of $c_\alpha(t)$ with a creation operator at one intermediate time and contraction of $c_\beta^\dagger(t')$ with an annihilation operator at different intermediate time can be performed in $4m(m-1)$ ways and one obtains

$$g^{(m)}_{\alpha\beta}(t-t') = \sum_{kr} \int_{-\infty}^{\infty} dt_{m-1} \int_{-\infty}^{\infty} dt_m g^{(0)}_{\alpha k}(t-t_{m-1}) \Bigg\{ \sum_{lmn;pqs} \frac{1}{2} V_{klmn} \Bigg[\frac{(-i)^{m-2}}{(m-2)!} \int_{-\infty}^{\infty} dt_1 \cdots \int_{-\infty}^{\infty} dt_{m-2} (-i) \times \langle \Phi_0 | T[H_1(t_1)\cdots H_1(t_{m-2}) c_l^\dagger(t_{m-1}) c_n(t_{m-1}) c_m(t_{m-1}) c_p^\dagger(t_m) c_q^\dagger(t_m) c_s(t_m)] | \Phi_0 \rangle \Bigg] \frac{1}{2} V_{pqrs} \Bigg\} g^{(0)}_{r\beta}(t_m - t'). \tag{13}$$

The expression between curly brackets is then recognized as the mth order reducible self-energy $\Sigma^{(m)}$ and can be written as

$$\Sigma^{(m)}_{\alpha\beta}(t-t') = \sum_{lmn;pqs} \frac{1}{2} V_{\alpha lmn} R^{(m-2)}_{mnl;pqs}(t-t') \frac{1}{2} V_{pq\beta s}, \tag{14}$$

in which $R^{(m-2)}$ is the $(m-2)$th order term in the perturbation expansion of the $2p1h$ propagator,

$$iR_{mnl;pqs}(t-t') = \langle \Psi_0^A | T[c_l^\dagger(t) c_n(t) c_m(t) c_p^\dagger(t') c_q^\dagger(t') c_s(t')] | \Psi_0^A \rangle. \tag{15}$$

This relation applies for all orders $m \geqslant 2$ in H_1.

In the irreducible self-energy Σ^*, one should leave out all diagrams in the perturbation expansion for R which fall apart in two pieces by cutting through a single fermion line. The first contribution to these reducible diagrams is of second order and is shown in Fig. 4. The expression for the nonstatic part of Σ^* is then [26]

$$\Sigma^*_{\alpha\beta}(\omega) = \sum_{lmn;pqs} \frac{1}{2} V_{\alpha lmn} \bar{R}_{mnl;pqs}(\omega) \frac{1}{2} V_{pq\beta s}, \tag{16}$$

where by $\bar{R}$ the part of R not containing reducible diagrams is meant. This quantity is referred to as the $2p1h$ response propagator [26].

One may note that if the zeroth order expression for $\bar{R}$,

$$\bar{R}^{(0)}_{123;1'2'3'}(\omega) = (\delta_{11'}\delta_{22'} - \delta_{12'}\delta_{21'})\delta_{33'} \Bigg\{ \frac{\theta(1-F)\theta(2-F)\theta(F-3)}{\omega - (\varepsilon_1+\varepsilon_2-\varepsilon_3) + i\eta} + \frac{\theta(F-1)\theta(F-2)\theta(3-F)}{\omega - (\varepsilon_1+\varepsilon_2-\varepsilon_3) - i\eta} \Bigg\}, \tag{17}$$

is used in Eq. (16), one obtains the familiar expression for the second order irreducible self-energy [Eq. (10)].

Approximations for Σ^* beyond second order can now be constructed by calculating $\bar{R}$ from an integral equation, which sums an infinite subset of diagrams for $\bar{R}$. In its most general form such an equation will be very difficult to deal with. The three-body vertex which connects two six-point Greens functions can in general depend on six time arguments. If, however, the restriction to two time arguments is made, thereby limiting the class of diagrams which could be summed by the equation, one solves, after Fourier transformation,

$$\bar{R}(\omega) = \bar{R}^{(0)}(\omega) + \bar{R}^{(0)}(\omega) K(\omega) \bar{R}(\omega), \tag{18}$$

with a certain choice for the vertex K. As a first approximation one can take the so-called [26] Faddeev or disconnected part or the three-body vertex K, which is the sum of three two-body vertices, one in the pp channel and two in the ph channels. The simplest case is when the two-body vertices are taken to be first order in the interaction. With this choice for K, Eq. (18) is graphically represented in Fig. 5.

With the methods known from the particle-particle and particle-hole cases [23], Eq. (18) can be cast into a secular equation, the so-called $2p1h$ TDA equation [27]

$$[\omega^{\nu}-(\varepsilon_1+\varepsilon_2-\varepsilon_3)]b^{\nu}_{123}=[\theta(1-F)\theta(2-F)\theta(F-3)-\theta(F-1)\theta(F-2)\theta(3-F)] \times\sum_{1'2'3'}\left\{V_{23'32'}\delta_{11'}+V_{13'31'}\delta_{22'}+\frac{1}{2}V_{121'2'}\delta_{33'}\right\}b^{\nu}_{1'2'3'}. \tag{19}$$

Note that in this equation the summation indices $1'2'3'$ satisfy the conditions that either $1'>F$, $2'>F$, $3'<F$ or $1'<F$, $2'<F$, $3'>F$; i.e., the correlations within the pph and hhp spaces are treated separately. From here on we will denote the restrictions on the three indices of the $2p1h$ response propagator by a string of three characters p or h and reserve the expression $2p1h$ for the general case. In mathematical expressions the three-character string enclosed by brackets will denote the collection of states with the restrictions given by the character string. The phase space factors give rise to a positive sign for $123\in\{pph\}$ and to a negative sign for $123\in\{hhp\}$. This resembles the fact that there is no sign difference between the forward and backward terms of the $2p1h$ response propagator [e.g., Eq. (17)], in contrast to the particle-particle and particle-hole propagators. In terms of the eigenvalues and eigenvectors of Eq. (19) the $2p1h$ response propagator is written as

$$\bar{R}_{123;1'2'3'}(\omega)=\sum_{\nu}\frac{b^{\nu}_{123}b^{\nu}_{1'2'3'}}{\omega-\omega^{\nu}} \tag{20}$$

and the corresponding expression for Σ^* becomes

$$\Sigma^*_{\alpha\beta}(\omega)=\sum_{\nu}\frac{[\Sigma_{123\frac{1}{2}}V_{\alpha312}b^{\nu}_{123}][\Sigma_{1'2'3'\frac{1}{2}}V_{1'2'\beta3'}b^{\nu}_{1'2'3'}]}{\omega-\omega^{\nu}}. \tag{21}$$

In Eqs. (20) and (21) the index ν denotes both the forward and the backward solutions of the $2p1h$ TDA equation. In the former case the summation indices in Eq. (21) run over the pph states, in the latter over the hhp states.

It should be noted that the first order Faddeev approximation does not contain the aforementioned reducible diagrams. Furthermore, no ground-state correlations are present in this approximation. In the present approach ground-state correlations appear if the vertex K contains also terms of second order in the interaction, which can connect the spaces of pph and hhp states, see Fig. 6. These correlations are, however, different from the ones usually considered at the two-body level in the pp or ph RPA. With the assumptions made in Eq. (18), it is not obvious how to include ground-state correlations at the two-body level in the $2p1h$ response propagator. In the next subsection we will discuss this further.

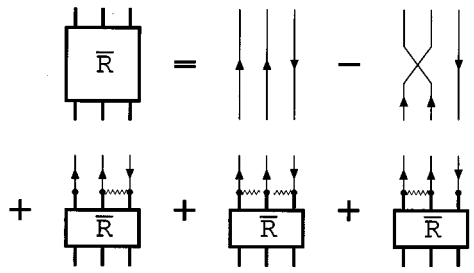

FIG. 5. Graphical representation of Eq. (18) with the first order Fadeev approximation for K.

From Eq. (19) it may be inferred that after omission of the two particle-hole vertices, one is left with essentially the pp TDA equation and $\bar{R}$ becomes

$$\bar{R}_{123;1'2'3'}(\omega)=\begin{cases}\Pi^{pp\mathrm{TDA}}_{12;1'2'}(\omega+\varepsilon_3)\delta_{33'} & (123,1'2'3'\in\{pph\}),\\ -\Pi^{pp\mathrm{TDA}}_{12;1'2'}(\omega+\varepsilon_3)\delta_{33'} & (123,1'2'3'\in\{hhp\}).\end{cases} \tag{22}$$

Similarly, omission of the particle-particle vertex and one of the particle-hole vertices reduces Eq. (19) to the ph TDA equation and leads to

$$\bar{R}_{123;1'2'3'}(\omega)=\begin{cases}\Pi^{ph\mathrm{TDA}}_{23;2'3'}(\omega-\varepsilon_1)\delta_{11'} & (123,1'2'3'\in\{pph\}),\\ -\Pi^{ph\mathrm{TDA}}_{23;2'3'}(\omega-\varepsilon_1)\delta_{11'} & (123,1'2'3'\in\{hhp\}).\end{cases} \tag{23}$$

Using these expressions in Eq. (16) is then a formal way to construct the self-energy approximations $\Sigma^{*pp\mathrm{TDA}}$ and $\Sigma^{*ph\mathrm{TDA}}$ used earlier [22].

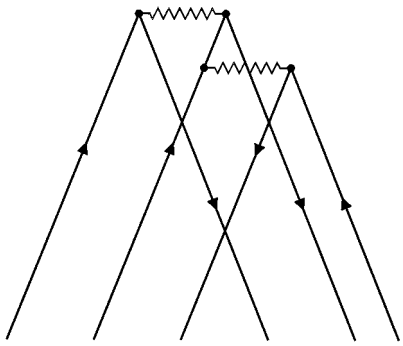

FIG. 6. Second order diagram for the vertex K of Eq. (18) which connects hhp and pph amplitudes of the $2p1h$ response propagator.

C. Extension with RPA-type two-particle–one-hole correlations

Since the RPA is more suitable to emphasize the collectivity of the (low energy) excitations, to which particle and hole motion couple, it is expected that the fragmentation of spectral strength at low energy and especially the occupation of orbits just above or below the Fermi level are better reproduced in an RPA type of approach for the $2p1h$ and $2h1p$ propagators. This will be illustrated for the hole spectral funnction of the (unoccupied) $f_{7/2}$ proton orbit in ^{48}Ca. The problem encountered with the inclusion of ground-state correlations at the two-body level in the $2p1h$ response propagator is that the restriction $1>F$, $2>F$, $3<F$ or $1<F$, $2<F$, $3>F$ for the indices is lifted. Instead the $2p1h$ response propagator has nonzero contributions for all eight possible combinations for the indices 123 to be below or above the Fermi level. The forward part of the $2p1h$ response propagator now has in addition to pph amplitudes also nonzero hhh amplitudes to account for ground-state correlations in the pp channel and nonzero php and hpp amplitudes to account for ground-state correlations in the ph channels. Similarly, the backward part of the $2p1h$ response propagator has in addition to hhp amplitudes also nonzero ppp, hph, and phh amplitudes. Because $\bar{R}^{(0)}$ does not exist for the quantum numbers 123 associated with these additional amplitudes, one needs a more general form of the integral equation than the one adopted in Eq. (18). Nevertheless, in Ref. [28], using the concept of mass operators for higher-point Green functions [29,30], the following secular equation was proposed:

$$[\omega^\nu-(\varepsilon_1+\varepsilon_2-\varepsilon_3)]\Gamma^\nu_{123}=\sum_{1'2'3'}\Big\{[\theta(F-3)-\theta(F-2)]V_{23'32'}\delta_{11'}+[\theta(F-3)-\theta(F-1)]V_{13'31'}\delta_{22'}$$
$$+[\theta(1-F)\theta(2-F)-\theta(F-1)\theta(F-2)]\frac{1}{2}V_{121'2'}\delta_{33'}\Big\}\Gamma^\nu_{1'2'3'}, \tag{24}$$

which differs from Eq. (19) only in the phase space factors. These phase space factors allow for the appearance of the additional amplitudes. The equation still separates into a forward part, which couples the pph space with the php, hpp, and hhh spaces, and a backward part which couples the hhp space to the hph, phh, and ppp spaces. The content of Eq. (24) becomes clear if the submatrices between the different spaces are written out explicitly. We will do this only for the forward part as the backward part goes the same way. For the forward part Eq. (24) then reads

$$\begin{pmatrix} A & B_1 & B_2 & B_3 \\ B_1^T & A_1 & & \\ B_2^T & & A_2 & \\ B_3^T & & & A_3 \end{pmatrix}\begin{pmatrix} X^\nu \\ X_1^\nu \\ X_2^\nu \\ X_3^\nu \end{pmatrix}=\omega^\nu\begin{pmatrix} 1 & & & \\ & -1 & & \\ & & -1 & \\ & & & -1 \end{pmatrix}\begin{pmatrix} X^\nu \\ X_1^\nu \\ X_2^\nu \\ X_3^\nu \end{pmatrix}, \tag{25}$$

with the submatrices and subvectors given by

$$\{A\}_{p_1p_2h_3;p_1'p_2'h_3'}=(\varepsilon_{p_1}+\varepsilon_{p_2}-\varepsilon_{h_3})\delta_{p_1p_1'}\delta_{p_2p_2'}\delta_{h_3h_3'}+V_{p_2h_3'h_3p_2'}\delta_{p_1p_1'}+V_{p_1h_3'h_3p_1'}\delta_{p_2p_2'}+\frac{1}{2}V_{p_1p_2p_1'p_2'}\delta_{h_3h_3'},$$

$$\{A_1\}_{p_1h_2p_3;p_1'h_2'p_3'}=-(\varepsilon_{p_1}+\varepsilon_{h_2}-\varepsilon_{p_3})\delta_{p_1p_1'}\delta_{h_2h_2'}\delta_{p_3p_3'}+V_{h_2p_3'p_3h_2'}\delta_{p_1p_1'},$$

$$\{A_2\}_{h_1p_2p_3;h_1'p_2'p_3'}=-(\varepsilon_{h_1}+\varepsilon_{p_2}-\varepsilon_{p_3})\delta_{h_1h_1'}\delta_{p_2p_2'}\delta_{p_3p_3'}+V_{h_1p_3'p_3h_1'}\delta_{p_2p_2'},$$

$$\{A_3\}_{h_1h_2h_3;h_1'h_2'h_3'}=-(\varepsilon_{h_1}+\varepsilon_{h_2}-\varepsilon_{h_3})\delta_{h_1h_1'}\delta_{h_2h_2'}\delta_{h_3h_3'}+\frac{1}{2}V_{h_1h_2h_1'h_2'}\delta_{h_3h_3'},$$

$$\{B_1\}_{p_1p_2h_3;p_1'h_2'p_3'}=V_{p_2p_3'h_3h_2'}\delta_{p_1p_1'},$$

$$\{B_2\}_{p_1p_2h_3;h_1'p_2'p_3'}=V_{p_1p_3'h_3h_1'}\delta_{p_2p_2'},$$

$$\{B_3\}_{p_1p_2h_3;h_1'h_2'h_3'}=\frac{1}{2}V_{p_1p_2h_1'h_2'}\delta_{h_3h_3'},$$

$$\{X^\nu\}_{p_1p_2h_3}=\Gamma^\nu_{p_1p_2h_3},\quad \{X_1^\nu\}_{p_1h_2p_3}=\Gamma^\nu_{p_1h_2p_3},$$

$$\{X_2^\nu\}_{h_1p_2p_3}=\Gamma^\nu_{h_1p_2p_3},\quad \{X_3^\nu\}_{h_1h_2h_3}=\Gamma^\nu_{h_1h_2h_3}. \tag{26}$$

The form $(\varepsilon_1+\varepsilon_2-\varepsilon_3)\delta_{11'}\delta_{22'}\delta_{33'}$ which is retained for the diagonal elements in the additional subspaces does not seem to make sense because, as stated earlier, $\bar{R}^{(0)}$ does not exist in these subspaces. One should therefore discard solutions which

have their greatest components in the additional subspaces as unphysical. This is immediately clear when the interaction is set to zero and Eq. (25) should yield the zeroth order approximation for $\bar{R}$, which exists only in the pph subspace. This observation was not made in Ref. [28].

The relevance of Eq. (25) can be checked by taking the limit where the interaction is considered in one channel only. If, for instance, only the interaction in the pp channel is considered, Eq. (25) reduces to

$$\begin{pmatrix} A & B_3 \\ B_3^T & A_3 \end{pmatrix} \begin{pmatrix} X^\nu \\ X_3^\nu \end{pmatrix} = \omega^\nu \begin{pmatrix} 1 & \\ & -1 \end{pmatrix} \begin{pmatrix} X^\nu \\ X_3^\nu \end{pmatrix}, \tag{27}$$

with the submatrix A now given by

$$\{A\}_{p_1p_2h_3;p_1'p_2'h_3'} = (\varepsilon_{p_1}+\varepsilon_{p_2}-\varepsilon_{h_3})\,\delta_{p_1p_1'}\delta_{p_2p_2'}\delta_{h_3h_3'} + \frac{1}{2} V_{p_1p_2p_1'p_2'}\delta_{h_3h_3'}. \tag{28}$$

The total matrix is now diagonal in the indices h_3 and $h_{3'}$. For each value of these indices Eq. (27) comprises a pp RPA eigenvalue equation. The eigenvalues corresponding to the physical and unphysical solutions of Eq. (27) are then easily recognized as

$$\omega^{\nu_{\rm phys}} = \omega_n^{A+2} - \varepsilon_{h_3}, \quad \omega^{\nu_{\rm unphys}} = \omega_n^{A-2} - \varepsilon_{h_3}, \tag{29}$$

where

$$\omega_n^{A\pm2} = \pm(E_0^{A\pm2} - E_0^A) \tag{30}$$

are the eigenvalues of the pp RPA equation. If furthermore the normalization condition

$$\sum_{123\in\{pph\}} \Gamma^\nu_{123}\Gamma^{\nu'}_{123} - \sum_{123\notin\{pph\}} \Gamma^\nu_{123}\Gamma^{\nu'}_{123} = \pm\,\delta_{\nu\nu'} \tag{31}$$

is adopted, the forward part of $\bar{R}(\omega)$ becomes

$$\bar{R}_{123;\,1'2'3'}(\omega) = \sum_n \frac{X^{A+2,n}_{12} X^{A+2,n}_{1'2'}}{\omega - (\omega_n^{A+2} - \varepsilon_3) + i\eta}\,\delta_{33'}, \qquad 123;1'2'3' \in \{pph\}\cup\{hhh\}, \tag{32}$$

where $X^{A+2,n}$ are the pp RPA eigenvectors corresponding to the eigenvalues ω_n^{A+2} of the pp RPA equation. When used in Eq. (16), this expression together with its equivalent for the backward part, will lead to the self-energy approximation $\Sigma^{*pp\rm RPA}$ of [22]. In a similar way, neglecting the interaction in the pp channel and in one of the ph channels in Eq. (25) will lead to the self-energy approximation $\Sigma^{*ph\rm RPA}$. Note that the normalization condition is different from the one given in Ref. [28]. Its form follows from the geometrical matrix in the right hand side of Eq. (25). A positive sign in Eq. (31) then indicates a physical solution and a negative sign an unphysical solution.

It should be noted that Eq. (25) is not a restatement of an integral equation, as is the case for the $2p1h$ TDA equation. This also implies that a diagramatic representation of the $2p1h$ RPA equation is not possible. The ground-state correlations at the two-body level are treated without considering a more complicated energy-dependent integral equation but at the expense of the appearance of unphysical solutions. The coupling of pp phonons and ph phonons takes place only at forward energies in the pph subspace whereas the additional subspaces serve to provide the phonons with their RPA character. If the additional subspaces are left out, Eq. (25) reduces to the $2p1h$ TDA equation.

The unphysical solutions should not be confused with the usual negative energy solutions of the pp or ph RPA equation. The backward part of the $2p1h$ RPA response propagator is given by the physical solutions of a separate equation in the hhp subspace extended with the hph, phh, and ppp subspaces.

Practical implementation of the $2p1h$ RPA equation in the case of medium heavy nuclei like ^{48}Ca and ^{90}Zr may be troublesome because of the huge dimension of the secular equation to be solved. The number of states to be considered for the $2p1h$ TDA equation [the submatrix A in Eq. (25)] is already several thousands and its solution reaches the practical limits of the possibilities of present mainframe computers. A partial solution of the $2p1h$ RPA equation, which will give the forward part of $\bar{R}(\omega)$ in the pph subspace only, is possible by treating the influence of coupling to the additional subspaces as an energy-dependent interaction in the pph subspace. We first rewrite Eq. (25) as a matrix inversion problem,

$$\bar{R}(\omega) = \begin{pmatrix} \omega - A & -B_1 & -B_2 & -B_3 \\ -B_1^T & -\omega - A_1 & & \\ -B_2^T & & -\omega - A_2 & \\ -B_3^T & & & -\omega - A_3 \end{pmatrix}^{-1}. \tag{33}$$

In the pph subspace $\bar{R}(\omega)$ is then given by

$$\bar{R}(\omega) = [\,\omega - A - K(\omega)\,]^{-1}, \tag{34}$$

with

$$K(\omega)=B_1\frac{1}{-\omega-A_1}B_1^T+B_2\frac{1}{-\omega-A_2}B_2^T+B_3\frac{1}{-\omega-A_3}B_3^T. \tag{35}$$

The inverses of the matrices $-\omega-A_1$, $-\omega-A_2$, and $-\omega-A_3$ are easily obtained as they are diagonal in one of the indices. They can be expressed as the TDA solutions in the hh and hp spaces,

$$\begin{aligned}
\left\{\frac{1}{-\omega-A_1}\right\}_{p_1h_2p_3;p_1'h_2'p_3'} &= \Pi^{ph\mathrm{TDA}}_{h_2p_3;h_2'p_3'}(\omega-\varepsilon_{p_1})\,\delta_{p_1p_1'},\\
\left\{\frac{1}{-\omega-A_2}\right\}_{h_1p_2p_3;h_1'p_2'p_3'} &= \Pi^{ph\mathrm{TDA}}_{h_1p_3;h_1'p_3'}(\omega-\varepsilon_{p_2})\,\delta_{p_2p_2'},\\
\left\{\frac{1}{-\omega-A_3}\right\}_{h_1h_2h_3;h_1'h_2'h_3'} &= \Pi^{hh\mathrm{TDA}}_{h_1h_2;h_1'h_2'}(\omega+\varepsilon_{h_3})\,\delta_{h_3h_3'}.
\end{aligned} \tag{36}$$

In terms of the TDA eigenvalues and eigenvectors, $K(\omega)$ is written as

$$\begin{aligned}
K_{p_1p_2h_3;p_1'p_2'h_3'}(\omega) = &-\sum_{\substack{h_2''p_3''\\ h_2'''p_3'''}} V_{p_2p_3''h_3h_2''}\sum_{n\neq 0}\frac{T^{A,n}_{h_2''p_3''}T^{A,n}_{h_2'''p_3'''}}{\omega-(\varepsilon_{p_1}-\omega_n^A)}V_{h_2'''h_3'p_3'''p_2'}\,\delta_{p_1p_1'}\\
&-\sum_{\substack{h_1''p_3''\\ h_1'''p_3'''}} V_{p_1p_3''h_3h_1''}\sum_{n\neq 0}\frac{T^{A,n}_{h_1''p_3''}T^{A,n}_{h_1'''p_3'''}}{\omega-(\varepsilon_{p_2}-\omega_n^A)}V_{h_1'''h_3'p_3'''p_1'}\,\delta_{p_2p_2'}\\
&-\sum_{\substack{h_1''h_2''\\ h_1'''h_2'''}} V_{p_1p_2h_1''h_2''}\sum_{n}\frac{T^{A-2,n}_{h_1''h_2''}T^{A-2,n}_{h_1'''h_2'''}}{\omega-(\omega_n^{A-2}-\varepsilon_{h_3})}V_{h_1'''h_2'''p_1'p_2'}\,\delta_{h_3h_3'}.
\end{aligned} \tag{37}$$

The $2p1h$ response propagator can now be calculated as a continuous function of the energy by direct matrix inversion of the right hand side of Eq. (34). This will, however, formally result in

$$\bar{R}_{p_1p_2h_3;p_1'p_2'h_3'}(\omega)=\sum_{\nu_{\mathrm{phys}}}\frac{\Gamma^{\nu_{\mathrm{phys}}}_{p_1p_2h_3}\Gamma^{\nu_{\mathrm{phys}}}_{p_1'p_2'h_3'}}{\omega-\omega^{\nu_{\mathrm{phys}}}}-\sum_{\nu_{\mathrm{unphys}}}\frac{\Gamma^{\nu_{\mathrm{unphys}}}_{p_1p_2h_3}\Gamma^{\nu_{\mathrm{unphys}}}_{p_1'p_2'h_3'}}{\omega-\omega^{\nu_{\mathrm{unphys}}}}=\bar{R}^{\mathrm{phys}}_{p_1p_2h_3;p_1'p_2'h_3'}(\omega)+\bar{R}^{\mathrm{unphys}}_{p_1p_2h_3;p_1'p_2'h_3'}(\omega), \tag{38}$$

and the separation of physical and unphysical solutions is no longer possible, particularly when the unphysical solutions appear in the same energy region as the physical ones. On the other hand, the unphysical solutions contribute through their components in the pph subspace only, which may be assumed to be small as long as the solutions are only moderately collective.

In the calculation of $\Sigma^*(\omega)$ with Eqs. (34) and (19) the energy is given a small imaginary part $\omega\rightarrow\omega+i\Delta$, to avoid singularities arising from the pole structure of $R(\omega)$ and $K(\omega)$. The hole spectral function is calculated by direct inversion of Eq. (5),

$$\begin{aligned}
S_h(\alpha,\omega) &= -\frac{1}{\pi}\,\mathrm{Im}\,g_{\alpha\alpha}(\omega)\\
&= -\frac{1}{\pi}\mathrm{Im}\left\{\frac{1}{g^{(0)-1}_{\alpha\alpha}(\omega)-\Sigma^*_{\alpha\alpha}(\omega)}\right\},
\end{aligned} \tag{39}$$

where for simplicity in the calculation the self-energy is taken to be diagonal.

The presence of unphysical solutions in the self-energy will give a negative contribution to the spectral strength. In the energy region where the physical solutions dominate the spectral strength, the calculation can be then justified by considering it as a lower estimate of the true spectral strength.

III. RESULTS FOR ^{48}Ca AND ^{90}Zr

The calculations presented in this section are performed with the same G-matrix interactions used in the calculations of Ref. [22]. The single-particle propagators are approximated by a single-pole expression with energies deduced from experiment. The procedure to assure the appearance of the largest single-particle strength fragment of the valence states at the experimental values is similar as in Refs. [9] and [22].

In the remainder of this section we will denote the ap-

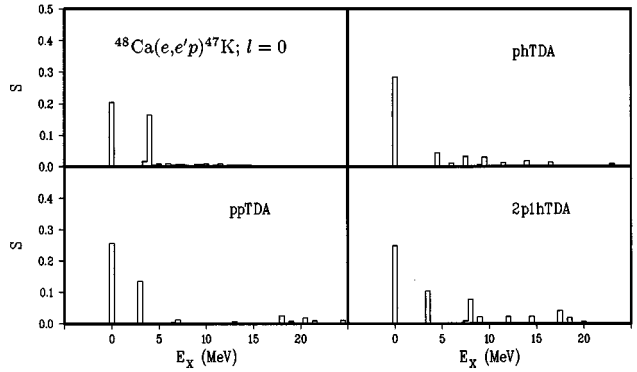

FIG. 7. The $2s$ hole spectral function of ^{48}Ca calculated with the ph TDA, pp TDA, and $2p1h$ TDA self-energy. The state at E_x=0.0 MeV has been reduced by a factor of 5 for plotting purposes. The experimental data are from Ref. [5].

proximation for the self-energy obtained by using the TDA approximation for the $2p1h$ response propagator in Eq. (16) as the $2p1h$ TDA self-energy. If the RPA approximation for the $2p1h$ response propagator is used, the resulting approximation for the self-energy will be denoted as the $2p1h$ RPA self-energy.

A. Results for ^{48}Ca with the $2p1h$ TDA self-energy

In Figs. 7 and 8 the $2s$ and $1d$ spectral functions, calculated with the $2p1h$ TDA self-energy, are displayed. In order to gain insight into the effects of the simultaneous coupling to pp and ph phonons in the self-energy, one should compare these results with the ph TDA and pp TDA results obtained earlier [22]. As mentioned before in Sec. II these are limiting cases of the more general $2p1h$ TDA approach in which the interaction is considered in only one of the three possible channels.

Special attention must be devoted to the removal of the spurious 1^- particle-hole excitation, resembling the coupling to the center of mass motion. When solving the $2p1h$ TDA equation, however, this solution will mix with other configurations and it will not be clear which solutions of the $2p1h$ TDA equation should be discarded. This problem was dealt

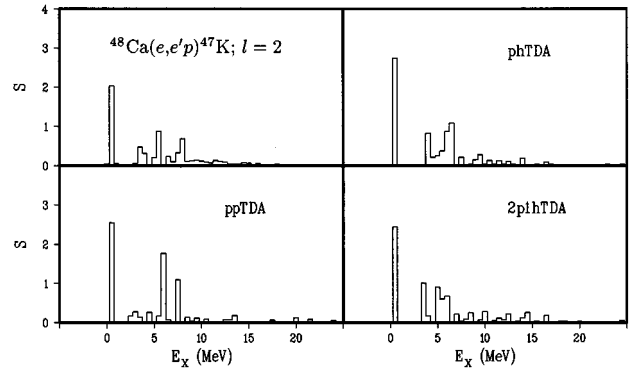

FIG. 8. The $1d$ hole spectral function of ^{48}Ca calculated with the ph TDA, pp TDA, and $2p1h$ TDA self-energy. The experimental data are from Ref. [5].

TABLE I. Spectroscopic factors of quasihole states in ^{47}K.

J^π	E (MeV)	Expt. [5]	$\Sigma^{*(2)}$	$\Sigma^{*ph\text{TDA}}$	$\Sigma^{*pp\text{TDA}}$	$\Sigma^{*2p1h\text{TDA}}$
$\frac{1}{2}^+$	0	1.07(7)	1.53	1.42	1.28	1.24
$\frac{3}{2}^+$	0.36	2.26(16)	2.94	2.75	2.56	2.45
$\frac{1}{2}^+$	3.85	0.167(14)	0.036	0.044	0.134	0.104

with by a method which shifts the spurious solutions sufficiently far away from the other solutions, so as to identify them easily. The details concerning this method are given in the Appendix.

From Table I it can be seen that the spectroscopic factors for the $\frac{1}{2}^+$ ground state and the $\frac{3}{2}^+$ state at 0.36 MeV of ^{47}K are somewhat smaller than in the pp TDA calculation, which gives the smallest values of the two TDA calculations. The $\frac{1}{2}^+$ at 3.85 MeV has a spectroscopic factor of 0.104 and lies in between the ph TDA and pp TDA result. This also applies for the summed spectroscopic strengths in the experimentally accessible regions listed in Table II.

The $1f$ spectral function is shown in Fig. 9. The considerable strength below 5.5 MeV found experimentally is still not quite reproduced, but the $2p1h$ TDA calculation does show an enhancement of strength in the low energy region compared with the calculations of Ref. [22]. Up to 5.5 MeV missing energy the $2p1h$ TDA calculation yields a summed strength of 0.21 whereas the ph TDA and pp TDA calculations yield 0.12 and 0.05, respectively, and the experimental value is 0.51(12).

The effect of the simultaneous coupling to pp and ph phonons in the self-energy seems more pronounced in the $1f$ spectral function than in the $2s$ and $1d$ spectral functions. This can be understood by examining the coupling of the single-particle states to the pph and hhp states which lie closest to the Fermi level. Because of parity and angular momentum conservation, these states are of different type for the occupied and unoccupied proton single-particle states. As a consequence of this, the simultaneous coupling to pp and ph phonons in the self-energy has a different effect on the positions of the poles of the self-energy just below and above the Fermi energy for the occupied and unoccupied proton single-particle states. The positions of these poles, listed in Table III for the valence shells and the various self-energy approximations, are important for describing the details of the spectral function at low values of the missing energy.

The hhp states closest to the Fermi level to which the $1f$ single-particle states couple are made up of two proton holes in the $2s1d$ shell and a proton particle in the $2p1f$ shell or a proton and a neutron hole in the $2s1d$ shell and a neutron particle in the $2p1f_{5/2}$ shell. The collective negative parity

TABLE II. Spectroscopic strengths in the experimental region for ^{48}Ca.

	$\Sigma^{*(2)}$	$\Sigma^{*ph\text{TDA}}$	$\Sigma^{*pp\text{TDA}}$	$\Sigma^{*2p1h\text{TDA}}$	Expt. [5]
$2s_{1/2}$					
$<$15.0 MeV	1.58	1.58	1.44	1.50	1.39(11)
$1d_{3/2+5/2}$					
$<$19.5 MeV	7.97	8.20	7.45	8.04	6.82(63)

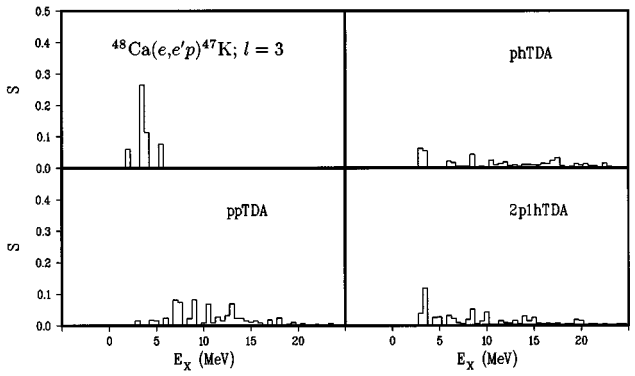

FIG. 9. The $1f$ hole spectral function of ^{48}Ca calculated with the ph TDA, pp TDA, and $2p1h$ TDA self-energy. The experimental data are from Ref. [5].

isoscalar ph phonons and the collective positive parity pp phonons in the $A-2$ nuclei have large components in this space. The mixing of these phonons by the $2p1h$ TDA equation moves the pole just below the Fermi energy of the backward part of the $2p1h$ response propagator towards the Fermi energy compared to the cases where only ph or pp phonons are included in the $2p1h$ response propagator. This explains the appearance of more $1f$ spectral strength in the low energy region.

The $2s$ and $1d$ single-particle states couple to the hhp states made up of a proton hole in the $2s1d$ shell, a neutron hole in the $1f_{7/2}$ level, and a neutron particle in the $2p1f_{5/2}$ shell. Other possibilities require particles or holes in more remote shells. Close to the Fermi level the density of hhp states to which the $2s1d$ single-particle states couple is smaller than for the $1f$ single-particle states. In the $2s1d$ case the space of hhp states close to the Fermi level contains also repulsive positive parity charge exchange ph phonons and the pole just below the Fermi energy of the $2p1h$ response propagator is now intermediate between the cases where only ph or pp phonons are considered.

For the forward part of the $2p1h$ response propagator the situation is reversed (see Table III). The combined effect is that for both the occupied and unoccupied proton single-particle states the gap in the self-energy is narrowed by about 1 MeV compared to the cases where only ph or pp phonons are included. This explains the reduction of the quasihole peaks of the $2s$ and $1d$ strength distributions.

At higher missing energies the simultaneous coupling to pp and ph phonons produces spectral functions somewhat intermediate between the ph TDA and pp TDA calculations. This can again be explained by the mixing of collective and repulsive phonons. Apart from the aforementioned summed spectroscopic strengths this is also visible from the total occupation numbers listed in Table IV.

TABLE III. Positions of self-energy poles around Fermi energy for ^{48}Ca.

	$1d_{3/2}$ $\varepsilon=-16.17$		$2s_{1/2}$ $\varepsilon=-15.81$		$1f_{7/2}$ $\varepsilon=-9.63$	
$\Sigma^{*(2)}$	−20.61	−3.45	−20.96	−3.45	−21.99	−4.83
$\Sigma^{*ph\text{TDA}}$	−20.01	−6.50	−20.37	−6.50	−18.94	−5.43
$\Sigma^{*pp\text{TDA}}$	−18.54	−4.46	−18.54	−4.82	−20.14	−6.36
$\Sigma^{*2p1h\text{TDA}}$	−19.38	−6.77	−19.22	−6.52	−18.63	−5.85

TABLE IV. Occupancies for ^{48}Ca.

Shell	$\Sigma^{*(2)}$	$\Sigma^{*ph\text{TDA}}$	$\Sigma^{*pp\text{TDA}}$	$\Sigma^{*2p1h\text{TDA}}$
$1s_{1/2}$	0.967	0.968	0.965	0.967
$1p_{3/2}$	0.955	0.956	0.950	0.952
$1p_{1/2}$	0.951	0.951	0.944	0.948
$1d_{5/2}$	0.920	0.925	0.898	0.918
$1d_{3/2}$	0.877	0.885	0.842	0.876
$2s_{1/2}$	0.869	0.860	0.818	0.836
$1f_{7/2}$	0.060	0.063	0.082	0.076
$1f_{5/2}$	0.048	0.044	0.064	0.051
$2p_{3/2}$	0.033	0.031	0.049	0.036
$2p_{1/2}$	0.030	0.028	0.042	0.033
$1g2d3s$	0.014	0.014	0.018	0.017
$1h2f3p$	0.006	0.006	00.007	0.006
Total	20.053	20.093	20.165	20.230

B. $1g_{9/2}$ hole spectral function for ^{90}Zr

As a further illustration of the $2p1h$ TDA self-energy is used in a calculation for the proton hole spectral function in ^{90}Zr. In this nucleus pairing correlations cause a partial occupation of the $2p_{1/2}$ and $1g_{9/2}$ shells and it is therefore of interest to see to what extend this method is applicable to such a situation. Because of the size of the $2p1h$ and $1h2p$ spaces, the TDA calculations had to be performed with one major shell fewer (i.e., five oscillator shells) than the aproximations pp TDA and ph TDA. In spite of this smaller model space, the $2p1h$ TDA calulation for the unoccupied $1g$ levels shows an enhancement of strength in the low energy region as compared to the aforementioned approximations. The results of these calculations are compared in Fig. 10 and in Tables V and VI. The experimental results are taken from Ref. [2]. The ph TDA and pp TDA calculations were performed in the larger model space.

Up to 5.75 MeV missing energy the summed spectroscopic strengths for the ph TDA and pp TDA are 0.33 and

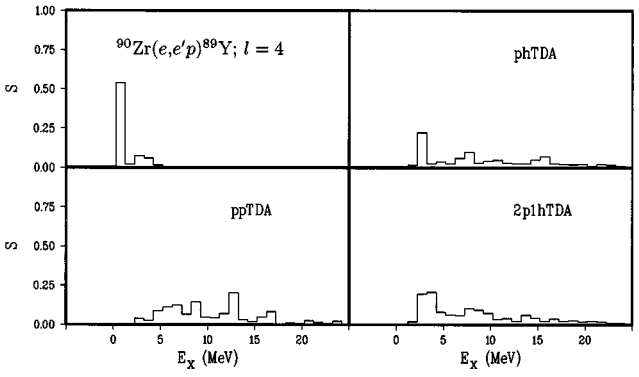

FIG. 10. The $1g$ hole spectral function of ^{90}Zr calculated with the ph TDA, pp TDA, and $2p1h$ TDA self-energy. Experimental data are taken from Ref. [2].

TABLE V. Spectroscopic factors of quasihole states in ^{89}Y.

J^π	E (MeV)	Expt. [2]	$\Sigma^{*(2)}$	$\Sigma^{*pp\mathrm{TDA}}$	$\Sigma^{*2p1h\mathrm{TDA}}$
$\frac{1}{2}^-$	0	0.72(7)	1.55	1.37	1.36
$\frac{3}{2}^-$	1.51	1.86(14)	3.08	2.67	2.68
$\frac{5}{2}^-$	1.75	2.77(19)	4.42	3.90	4.02

0.27, respectively. The $2p1h$ TDA result is 0.56, as compared to the experimental value of 0.71.

C. Extension to $2p1h$ RPA self-energy

As explained in Sec. II C the use of the $2p1h$ RPA is beset with problems, notably the lack of a clear separation between physical and unphysical solutions. This separation, where possible at all, is further obscured by the method of direct matrix inversion with the effective $K(\omega)$ as embodied in Eqs. (34) and (35). This method must be used because otherwise the dimensions of the numerical problem become prohibitive. For the same reason we implemented the RPA only for the backward (hole) part of the $2p1h$ reponse propagator, in an attempt to get an impression of the relevance of an RPA-type extension of the $2p1h$ TDA method appplied here. An advantage of the treatment via the construction of the effective $K(\omega)$ is that it is possible to identify contributions from unstable RPA solutions such as, e.g., the 3^- in the ph RPA. These 3^- are then replaced by their Tamm-Dancoff counterparts. In this way we obtain a partial RPA-type extension of the $2p1h$ TDA propagator, avoiding some of the problematic RPA features.

The relevance of such an extension for the hole spectral function of orbits above the Fermi level is illustrated in Fig. 11 for the $1f$ proton hole strength, calculated as a continuous distribution according to Eq. (39). For comparison the $2p1h$ TDA result is also shown as a continuous distribution. The energy distribution is computed with an imaginary part of 0.25 MeV. Note that the RPA strength distribution will become negative for missing energies lower than 0.5 MeV. In this energy region the self-energy has only poles corresponding to the unphysical solutions of the $2p1h$ RPA equation. Although their strength is small, they will give a wrong energy behavior for the self-energy and the spectral function. For larger values of the missing energy the stronger physical solutions dominate and the spectral strength distribution is positive everywhere. It should be remarked, however, that the influence of the unphysical $2p1h$ RPA solutions could have become large here as well, if the RPA $2p1h$ had also been applied for the forward part of the $2p1h$ propagator. So a straightforward application of some form of the $2p1h$ RPA is only possible after a method has been found to avoid or remove the unphysical solutions, discussed in Sec. II C.

TABLE VI. Spectroscopic strengths in the experimental region for ^{90}Zr.

	$\Sigma^{*(2)}$	$\Sigma^{*pp\mathrm{TDA}}$	$\Sigma^{*2p1h\mathrm{TDA}}$	Expt. [2]
$1f_{5/2+7/2}$ <21.0 MeV	11.44	10.85	11.34	8.75(63)
$2p_{1/2+3/2}$ <7.0 MeV	4.76	4.39	4.30	2.97(15)

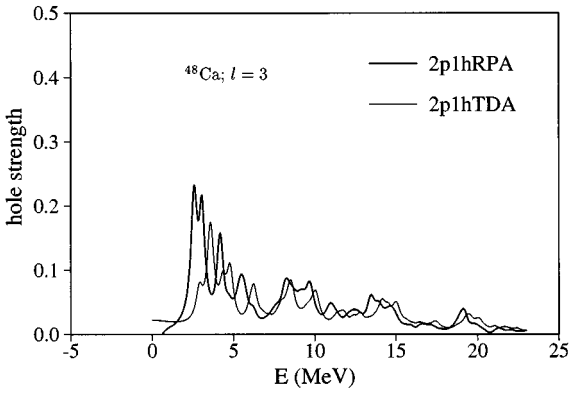

FIG. 11. The $1f$ hole spectral function of ^{48}Ca calculated with the $2p1h$ TDA (thin line) and $2p1h$ RPA self-energy (thick line).

The RPA calculation shows a further enhancement of strength at low energies. The strength up to 5.5 MeV missing energy is now 0.41, nearly twice the strength obtained with the $2p1h$ TDA method and closer to the experimental value 0.51(12). The value of the RPA calculation is derived by fitting the strength distribution with a sum of Lorentzians, which is the formal expression for a spectral function when the energy has a finite imaginary part. At higher values of the missing energy the RPA distribution is rather similar to the TDA result.

The calculation shows that the effects of coupling of pp and ph collective modes is more pronounced if ground-state correlations are included. Compared with the $2p1h$ TDA approach the ground-state correlations induce an extra energy-dependent interaction $K(\omega)$. The energy dependence of $K(\omega)$ assures a stronger coupling of phonons in configurations where the interaction is attractive in both the pp and ph channels, which is the case for the hhp states to which the $1f$ single-particle levels couple at low energy. At higher energies this effect is compensated by mixing with phonons which become more repulsive in the RPA.

IV. SUMMARY AND CONCLUSIONS

The combined effect of particle-particle and particle-hole correlations on the proton self-energy and the associated hole spectral function is investigated by employing the relation between the self-energy and the two-particle–one-hole ($2p1h$) response propagator. The latter was treated in a Tamm-Dancoff approximation, with proton hole states in ^{48}Ca and the $1g$ orbit in ^{90}Zr as illustrative examples. A realistic G-matrix interaction [9] deduced from the Bonn potential was used.

For unoccupied proton levels it was found that simultaneous coupling to particle-particle and particle-hole collective modes moves the lower edge of the gap in the self-energy towards the Fermi energy. An enhancement of spectral strength at low values of the missing energy then results for these levels as compared to methods where either particle-particle or particle-hole collective modes are included in the self-energy. The amount of strength in this region is, however, still less than found experimentally.

For both occupied and unoccupied proton levels the simultaneous coupling to particle-particle and particle-hole collective modes narrows the gap in the self-energy and the spectroscopic factors of the quasihole states are reduced.

The details of spectral strength distributions at low energy are intimately related to the low-energy behavior of the $2p1h$ response propagator. In this energy region a description of the $2p1h$ response propagator beyond a factorization in a correlated two-body propagator and a spectator one-body propagator is essential. At the lowest energies, where collective features may be most pronounced, the replacement of a Tamm-Dancoff by a RPA-correlated propagation can make a big difference. Especially the description of hole strength for orbits above the Fermi level seems to require the application of such methods.

Straightforward application of a method known in the literature as $2p1h$ RPA is not possible, however, because of unsolved problems with a multitude of unphysical solutions that cannot simply be identified and removed. A reformulation of the $2p1h$ RPA in a way that avoids these problems is an important point of further investigation.

ACKNOWLEDGMENTS

This work is part of the research program of the Foundation for Fundamental Research of Matter (FOM), which is financially supported by the Netherlands' Organization for Scientific Research (NWO). It was also partially supported by the U.S. National Science Foundation under Grant No. PHY-9301484 (at Washington University). Computer time was supplied by the Netherlands' Foundation for National Computer Facilities (NCF).

APPENDIX

In principle one should project the spurious 1^- ph TDA phonon out of the pph space [27]. In order to avoid the complications involved with this procedure the following method was considered. The ph TDA equation

$$\sum_{p_1'h_2'} \{(\varepsilon_{p_1}-\varepsilon_{h_2})\delta_{p_1p_1'}\delta_{h_2h_2'}+V_{p_1h_2',h_2p_1'}\}X^{A,n}_{p_1'h_2'} = \omega^A_n X^{A,n}_{p_1h_2} \tag{A1}$$

is modified by adding to the interaction in the 1^- ph channel a two-body operator W, the matrix elements of which in the ph space obey

$$\sum_{p_1'h_2'} W_{p_1h_2',h_2p_1'}X^{A,n}_{p_1'h_2'}=0 \tag{A2}$$

if $n\neq n_{\text{spurious}}$ and

$$\sum_{p_1'h_2'} W_{p_1h_2',h_2p_1'}X^{A,n\ \text{spurious}}_{p_1'h_2'}=E_{shift}X^{A,n\ \text{spurious}}_{p_1h_2} \tag{A3}$$

for the spurious solution.

With W added to the interaction in the 1^- ph channel, the ph TDA equation will yield unaltered eigenvectors and eigenvalues ω^A_n for $n\neq n_{\text{spurious}}$. The eigenvalue of the spurious solution, however, will be shifted upwards in energy by an amount E_{shift}. In the calculations $E_{\text{shift}}=300$ MeV is adopted. The matrix elements of W can be found from

$$X^TWX=D, \tag{A4}$$

where X is the matrix of eigenvectors,

$$X=(\cdots,X^{A,i},\cdots,X^{A,n_{\text{spurious}}}) \tag{A5}$$

and D the diagonal matrix with the eigenvalues of W,

$$D=\begin{pmatrix} \ddots & & \\ & 0 & \\ & & \ddots \\ & & & E_{\text{shift}} \end{pmatrix}. \tag{A6}$$

From Eq. (A4) one finds for W

$$W=XDX^T. \tag{A7}$$

When the modified interaction is used in the $2p1h$ TDA equation one or more solutions will appear at much higher (in the forward case) or much lower (in the backward case) energy. These solutions are discarded as they consist for a major part of the spurious 1^- ph TDA phonon. The mixing of the 1^- ph TDA phonon in the other solutions can then be assumed to negligible due to the large difference in energy.

[1] S. Frullani and J. Mougey, Adv. Nucl. Phys. **14**, 1 (1984).
[2] J. W. A. den Herder *et al.*, Nucl. Phys. **A490**, 507 (1988).
[3] P. K. A. de Witt-Huberts, J. Phys. G **16**, 507 (1990).
[4] G. van der Steenhoven, Nucl. Phys. **A527**, 17c (1991).
[5] G. J. Kramer, Ph.D. thesis, NIKHEF, Amsterdam, 1990.
[6] C. Mahaux and H. Ngo, Phys. Lett. **100B**, 285 (1981).
[7] C. Mahaux and R. Sartor, Nucl. Phys. **A503**, 525 (1989).
[8] C. Mahaux and R. Sartor, Nucl. Phys. **A528**, 253 (1991).
[9] M. G. E. Brand *et al.*, Nucl. Phys. **A531**, 253 (1991).
[10] I. Sick and P. K. A. de Witt-Huberts, Comments Nucl. Part. Phys **20**, 177 (1991).
[11] M. Leuschner *et al.*, Phys. Rev. C **49**, 955 (1994).
[12] O. Benhar, C. C. degli Atti, S. Lutti, and G. Salmé, Phys. Lett. B **177**, 135 (1986).
[13] A. Ramos, A. Polls, and W. Dickhoff, Nucl. Phys. **A503**, 1 (1989).
[14] B. E. Vonderfecht, W. H. Dickhoff, A. Polls, and A. Ramos, Nucl. Phys. **A555**, 1 (1993).
[15] O. Benhar, A. Fabrocini, and S. Fantoni, Nucl. Phys. **A505**, 267 (1989).
[16] O. Benhar, A. Fabrocini, and S. Fantoni, Phys. Rev. C **41**, R24 (1990).
[17] H. Müther and W. H. Dickhoff, Phys. Rev. C **49**, R17 (1994).
[18] D. van Neck, A. E. L. Dieperink, and E. Moya de Guerra, Phys. Rev. C **51**, 1800 (1995).

[19] W. H. A. Hesselink and E. Jans, NIKHEF-K electron scattering proposal No. **94-1**, 1994.
[20] L. J. H. M. Kester *et al.*, Phys. Rev. Lett. **74**, 1712 (1995).
[21] D. van Neck, M. Waroquier, and J. Ryckebusch, Nucl. Phys. **A530**, 347 (1991).
[22] G. A. Rijsdijk, K. Allaart, and W. H. Dickhoff, Nucl. Phys. **A550**, 159 (1992).
[23] A. L. Fetter and J. D. Walecka, *Quantum Theory of Many Particle Physics* (McGraw-Hill, New York, 1971).
[24] A. A. Abrikosov, L. P. Gorkov, and I. E. Dzyaloshinski, *Methods of Quantum Field Theory in Statistical Physics* (Dover, New York, 1963).
[25] P. C. Martin and J. Schwinger, Phys. Rev. **115**, 1342 (1959).
[26] J. Winter, Nucl. Phys. **A194**, 535 (1972).
[27] P. Ring and P. Schuck, Z. Phys. **269**, 323 (1974).
[28] P. Schuck, F. Villars, and P. Ring, Nucl. Phys. **A208**, 302 (1973).
[29] G. F. Mazenko, Phys. Rev. A **6**, 2545 (1972).
[30] P. Schuck, Z. Phys. **241**, 395 (1971).